Boron Cluster Lamellar Phases

DOI: 10.1002/ange.201307357

Lyotropic Lamellar Phase Formed from Monolayered θ-Shaped Carborane-Cage Amphiphiles**

Damien Brusselle, Pierre Bauduin, Luc Girard, Adnana Zaulet, Clara Viñas, Francesc Teixidor, Isabelle Ly, and Olivier Diat*

Lyotropic lamellar phases occur naturally and are a key architectural feature for life to develop as they enable the formation of closed-cell topologies.[1] But in addition to closed-cell topologies, enabling life means that the same solvent must be on both sides of the cell membrane, hence at least a double-layered membrane structure is necessary. For this a lamellar phase must be enabled. Herein we show that the formation of lamellar phases is not exclusive to alkyl-chain-based surfactants with a well-defined amphiphilic structure but that it can also be obtained with metallacarborane clusters, described previously as θ-shaped amphiphiles.[2] Similarly to phospholipid cell membranes the lamellae formed can exist both in the liquid and in the solid states depending on temperature. The determination of the 2D molecular arrangement in the lamella demonstrated that the formation of intermolecular dihydrogen bonds, such as -C-$H^{\delta+}$...$^{\delta-}$H-B-, is the driving force in the lamella self-assembly process. Compared to the common bilayer structure that originates from the hydrophobic effect,[3] θ-shaped amphiphiles form lamellae with a peculiar monomolecular structure reminiscent of lamellar sheets observed in inorganic layered systems.[4] Nano-scale ordering of planar organic–inorganic hybrid sheets is controlled by temperature and concentration through a self-assembly process.

The lyotropic lamellar phase, characterized by an elementary smectic liquid-crystal symmetry, is by far the most common surfactant mesophase.[5] A vast literature can be found on the topic as it shows practical applications in many different fields, such as in detergents, pharmaceutics,[6] food,[7] or materials synthesis as templates.[8] Its mesostructure consists of parallel stacks of bilayers, the structural unit of biological membranes, separated by water layers. To distinguish between molten and frozen states of the surfactant alkyl chains, lamellar phases are referred to as L_α and L_β (or "gel phase").[9] Therefore the surfactant has a liquid-like mobility in L_α whereas chain motions are highly restricted in L_β, mostly limited to rotation about the chain axis as is the case in rotator phases formed in long-chain alkanes. Surfactants in the bilayers have mostly an *all-trans* alkyl-chain conformation with possible chain inter-digitation or chain tilt in the case of L_β. Lyotropic lamellar phases have only been observed with molecules that have a well-defined amphiphilic character.

Herein, we show that metallabis(dicarbollide derivatives),[10] large anions with amphiphilic properties, form lyotropic lamellar phases at high concentrations in water. In previous studies, the surfactant-like properties of cobaltabis(-dicarbollide) anion ($[COSAN]^-$ with H^+ as the counterion) were highlighted.[2,11] Even though the central region of $[COSAN]^-$ around the cobalt atom is more polar (and locally charged) than its two extremities,[12] H[COSAN] (Figure 1) does not show a classical amphiphilic structure and was therefore named θ-shaped amphiphile in reference to its molecular shape. H[COSAN] self-assembles in water by forming isotropic phases: vesicles of monomolecular thickness in diluted regime that turn into small micelles by increasing concentration.

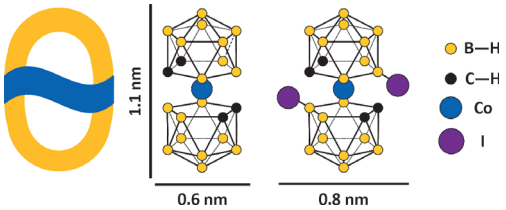

Figure 1. Chemical structure of the amphiphilic ion, $[COSAN]^-$ (left), and its diiodinated derivative, $[I_2COSAN]^-$ (right) whose shape is compared to the Greek letter θ (far left).

We focus herein on the diiodo-COSAN ($[I_2COSAN]^-$ with H^+ as counterion, Figure 1) by determining the temperature–concentration (T/ϕ) phase diagram[13] of the binary system with water that shows the occurrence of anisotropic birefringent phases (Figure 2). By combining visual observa-

[*] D. Brusselle, Dr. P. Bauduin, Dr. L. Girard, Dr. O. Diat
ICSM, UMR 5257 (CEA, CNRS, UM2, ENSCM)
CEA Marcoule
BP 17171, 30207 Bagnols-sur-Cèze (France)
E-mail: Pierre.Bauduin@cea.fr
A. Zaulet, Prof. C. Viñas, Prof. F. Teixidor
ICMAB (CSIC)
Campus de la UAB 08193 Bellaterra (Spain)
I. Ly
Centre de Recherche Paul Pascal (CRPP)
CNRS 115 av. Schweitzer F-33600 Pessac (France)

[**] This work was supported by the Presidency and the scientific committee of the University of Montpellier II. We would like to thank O. Mondain-Monval, J. Cambedouzou, S. Prevost, J.C. Gabriel, and Th. Zemb for fruitful discussions on, respectively, the interpretation of the TEM pictures, on the 2D-crystallographic structure determination, on small-angle scattering data (and production of the 3D graphical artwork) and on the properties of rigid bilayers. Bruno Corso was very helpful for technical support with the SWAXS apparatus. This research has been financed by MEC (CTQ 2010-16237) and Generalitat de Catalunya (2009/SGR/00279). A.Z. is enrolled in the Ph.D. program of the UAB.

Supporting information for this article is available on the WWW under http://dx.doi.org/10.1002/anie.201307357.

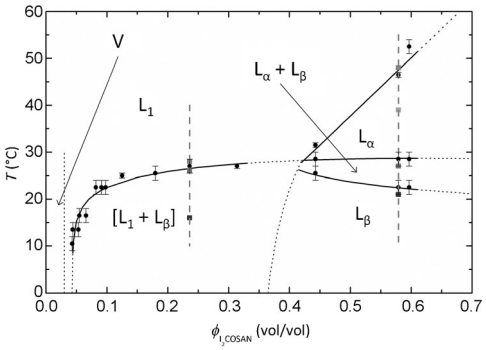

Figure 2. Binary phase diagram of H[I_2COSAN] in water showing the existence of lamellar lyotropic phases, L_α and L_β, isotropic micellar (L_1) and vesicular (V) phase. [$L_1 + L_\beta$] refers to a "gel" phase being a microscopic demixion of L_1 and L_β. Round data points correspond to experimental transition phase limits. The vertical dashed lines correspond to the samples at the two concentrations considered in Figure 4 concerning the SAXS study at different temperatures (squares).

tions, dynamic and static light scattering (DLS/SLS), small- and wide-angle X-ray scattering (SWAXS), $^{11}B\{^1H\}$ NMR spectroscopy, polarized optical light microscopy (POM) and freeze-fracture electron microscopy (FF-TEM), several ordered and disordered phases were identified over a large range of temperature and concentration.

In the diluted regime, H[I_2COSAN] is found to behave similarly as H[COSAN] by forming vesicles with a radius of gyration of around 98.3 nm as determined by DLS/SLS (see Supporting information, Figure S1). At high concentrations above 35% v/v, optical microscopy pictures show birefringence with the presence of Maltese crosses (left side in Figure 3a) that are typical of lamellar phases. Applying a soft shear stress, by sliding the microscopy slide cover slip, the system can be easily mechanically aligned over one centimeter square (right side of Figure 3a). At temperatures below

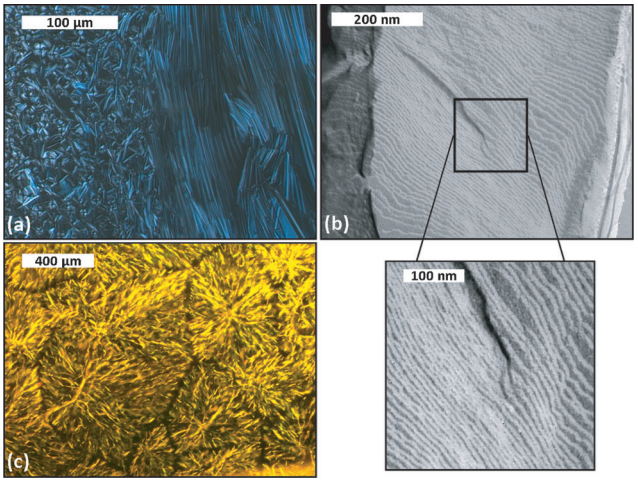

Figure 3. a) Polarized optical microscope images of the "gel" phase [$L_1 + L_\beta$], b) freeze-fracture TEM picture of the pure L_β phase showing the lamellar arrangement with an apparent inter-lamellar distance of roughly 5 nm confirmed by SWAXS, and c) optical microscope picture showing a spherulite texture of the "gel" phase [$L_1 + L_\beta$].

20 °C and volume fractions above 40% SWAXS spectra show in the low q-range a series of diffraction peaks with a 1:2:3:4 … ratio which is a signature of a lamellar ordering (see the spectrum at 21 °C in Figure 4b) that confirms the microscopy observation. The occurrence of many sharp peaks in the large q-range, above 8 nm^{-1} indicates a supplementary solid-like molecular ordering typical of L_β phase. By increasing temperature above 27 °C, these Bragg peaks turn into a broad peak centered at 9.7 nm^{-1} ($d = 0.65$ nm) characteristic of the melting effect within the lamella. The H[I_2COSAN] molecules of the layers undergo here a transition from solid- to fluid-like behavior which is the characteristic of a L_β to L_α transition. This transition was confirmed by $^{11}B\{^1H\}$ NMR spectra of 1 M solution of H[I_2COSAN] in water as function of T °C, see Figure S2. Between 20 and 27 °C two series of Bragg peaks in the low q regime are observed (see Figure 4b at 27 °C) indicating that L_β and L_α phases coexist and that the transition is first order. The lamella thickness (δ) can be estimated from d^* values, the periodicity of the lamellar structure, and the [I_2COSAN]$^-$ volume fraction, ϕ, with $d^* = \delta/\phi$. δ lies between 1.1 and 1.4 nm which is in the order of the molecular length (ca. 1.1 nm for the molecular long axis). Therefore the lamellae are made of monomolecular layers with the H[I_2COSAN] molecules oriented orthogonally to the lamella plane. It has already been shown that H[COSAN] adopts such a molecular arrangement in the wall structure of vesicles formed in the diluted regime.[2] By increasing further the temperature, the solution becomes isotropic with no birefringence and is referred to as the micellar phase, L_1.

At intermediate concentrations, between around 4–5% (around 100 mM) and 40% v/v a stable highly viscous "gel" is observed at temperatures below 25 °C. Optical microscopy shows birefringent micrometric inhomogeneity ("hairy-like") with a large millimetric spherullitic texture (Figure 3c) which is commonly observed during crystallization of polymer melts in highly ordered lamellar regions.[14] SWAXS spectra in this concentration regime also show a series of diffraction peaks with a 1:2:3:4… ratio in the low q values and Bragg peaks in the large q domain, above 8 nm^{-1}, as in the pure L_β phase (Figure 4b). However, the SWAXS spectra differ from the one observed with the L_β at higher concentrations. A broad peak is superimposed on the scattering curves and presents a maximum intensity at q values around 1 nm^{-1}, depending on concentration. This contribution to the scattered intensity can be attributed to the presence of nano-aggregates as it was previously concluded for H[COSAN] in a similar concentration range.[2] These aggregates were described in a first approximation as small spherical micelles with an average aggregation number of approximately 12 and with a radius of around the length of the COSAN$^-$ ion that is, 1.1 nm. Increasing temperature induces the melting of the gel in a pure isotropic micellar phase, L_1 (Figure 2). This transition is concomitant with the disappearance of the lamellar signature in the SWAXS spectra, leaving only the micelle signal (Figure 4a, upper curve).[2] Consequently the "gel" phase is made of a mixture of L_1 and L_β phases dispersed in micro-domains that do not phase separate macroscopically. Such local segregations of two distinct phases, lamellar and diluted phases, on a colloidal scale has been observed with

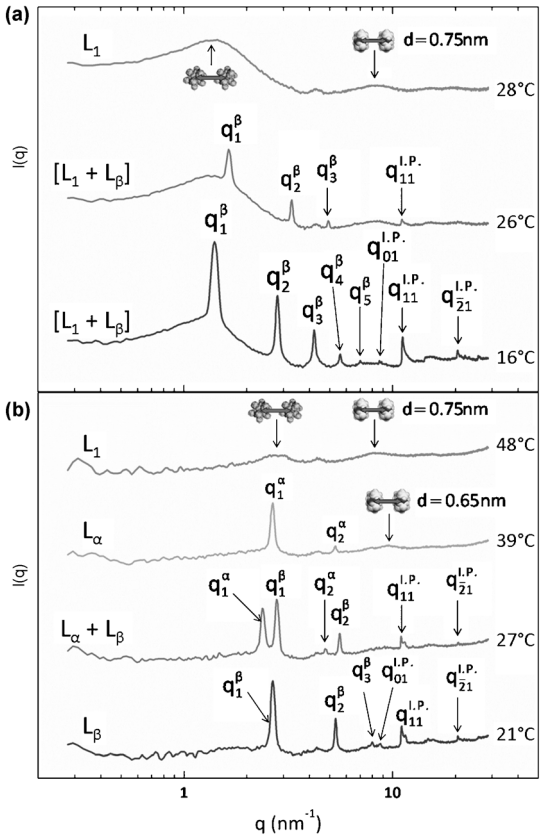

Figure 4. SWAXS spectra of H[I_2COSAN] in water at different temperatures at a) 23.5 and b) 59% v/v.

some double-chained surfactant systems[15] as well as in purely inorganic clay systems forming the so-called tactoids.[16] For surfactant systems the notation $[L_1+L_\beta]$ or $[L_\beta]$ is commonly used to refer to such $L_\beta+L_1$ dispersions.

The inter-lamellar distance (d^*) in the L_β micro-domains of the $[L_1+L_\beta]$ phase can also be calculated from the position of the first order peak in SWAXS spectra such as $d^*=2\pi/q$. Dilution, as well as a decrease in temperature, leads to exfoliation (or swelling) of the lamellae whose periodicity range from approximately 2 up to around 7 nm that corresponds to the maximum swelling (Figure S3). Pictures of the lamellar arrangement in the L_β phase obtained by freeze-fracture transmission electron microscopy (FF-TEM) confirm the 1D long range ordering of the lamella as inferred from the sharpness of the peaks observed in SWAXS as well as the order of magnitude of d^* (Figure 3b). Swelling of layered systems is a general process observed for example during the dilution of lamellar phases made of surfactants, inorganic covalently bound sheets such as clays[17] or other systems made of phosphatoantimonate layers.[18]

At constant temperature in the $[L_1+L_\beta]$ region d^* continuously decreases by increasing H[I_2COSAN] concentration (Figure S3) whereas the intensity of the micelles signal, which is related to the micelle concentration, decreases (Figure S4). Therefore the compositions in the micro-phases change continuously while the concentration varies. As a consequence, the biphasic $[L_1+L_\beta]$ region does not represent the case of a macroscopic phase separation with identified tie lines. For a macroscopic phase separation between a lamellar phase and a second liquid phase the osmotic equilibrium condition, that is, $|\pi_1-\pi_2|=0$ with π_i the osmotic pressures in the two phases in equilibrium, sets the spacing observed between the lamellae.[19] In the present case the interfacial energy of contact between the two micro-phases cannot be neglected in the thermodynamic analysis leading to the master equation $|\pi_{L\beta}-\pi_{L1}|=\gamma A$ with γ and A the interfacial tension and specific surface between the micro-phases respectively. For macroscopic dispersions, the large size of the domains leads to small specific surfaces and to a negligible contribution of the interfacial energy resulting in a constant d^* value along a given tie line when concentration is varied. Consequently, the variation in d^* observed at constant temperature can be explained by considering a significant contribution of the interfacial energy between the micro-phases.[15]

To go further in the determination of the lamella molecular organization, the position of the three main Bragg peaks observed at around 8.6, 11.2, and 20.5 nm^{-1} (Figure 4) in the pure L_β and in the biphasic $[L_1+L_\beta]$ phases can be analyzed. These peaks correspond to the diffraction of crystallographic planes within the monolayer (in-plane diffraction peaks noted $q^{I.P.}$), as inferred from the saw-tooth shape of the peaks,[20] while the diffraction peaks (q^α or q^β) observed at lower q values correspond to out-of-plane diffraction. The peaks positions could be well indexed with an oblique lattice, with lattice parameters $a=b=7.4$ Å and $\theta=80.5°$, which is one of the five types of the 2D Bravais lattices. The peaks in the SAXS spectra were then indexed according to the crystallographic planes (01) or (10), (11), and ($\bar{2}1$), respectively, for the first, second, and third peak observed. We can thus propose a 2D lattice of the lamellae, as shown in Figure 5, which is in good agreement with the molecular distances with one $[I_2COSAN]^-$ ion per lattice. In this structure it was considered that $[I_2COSAN]^-$ ions present a twofold symmetry with the two iodine atoms in *trans* position, as shown in Figure 1, which represents the most stable rotamer, that is, *transoid*, as supported by the crystal structures (codes DEXPIF, IHOHAP, IHOHET, and IHOHIX) in the Cambridge Structural Database. The 2D arrangement shows that $[I_2COSAN]^-$ ions are not in close contact but are separated by a distance of 3.5 Å that may be due to the presence of intermolecular dihydrogen bonds, such as -C-$H^{\delta+}$...$^{\delta-}$H-B- or B-$H^{\delta+}$...$^{\delta-}$H-B, reducing the energy of the crystal. Such dihydrogen bonds are observed in the solid state for the [BEDT-TTF][I_2COSAN] (CSD code IHOHAP)[21] which has dihydrogen B-$H^{\delta+}$...$^{\delta-}$H–B bonds of 3.500 Å matching the value found in our case (Figure S7). According to the 2D structure, it is then likely that the self-assembly process of $[I_2COSAN]^-$ ions in monomolecular lamella relies on a network of such H-bonds while the formation of bilayers with classical surfactants is mainly driven by the hydrophobic effect. Interestingly the molecular area occupied by a $[I_2COSAN]^-$ ion in the monolayer decreases from 53.9 $Å^2$, that is, the area of the 2D crystal lattice, in the L_β phase, to 43 $Å^2$ in the L_α phase. This latter surface area was calculated as the square of the average

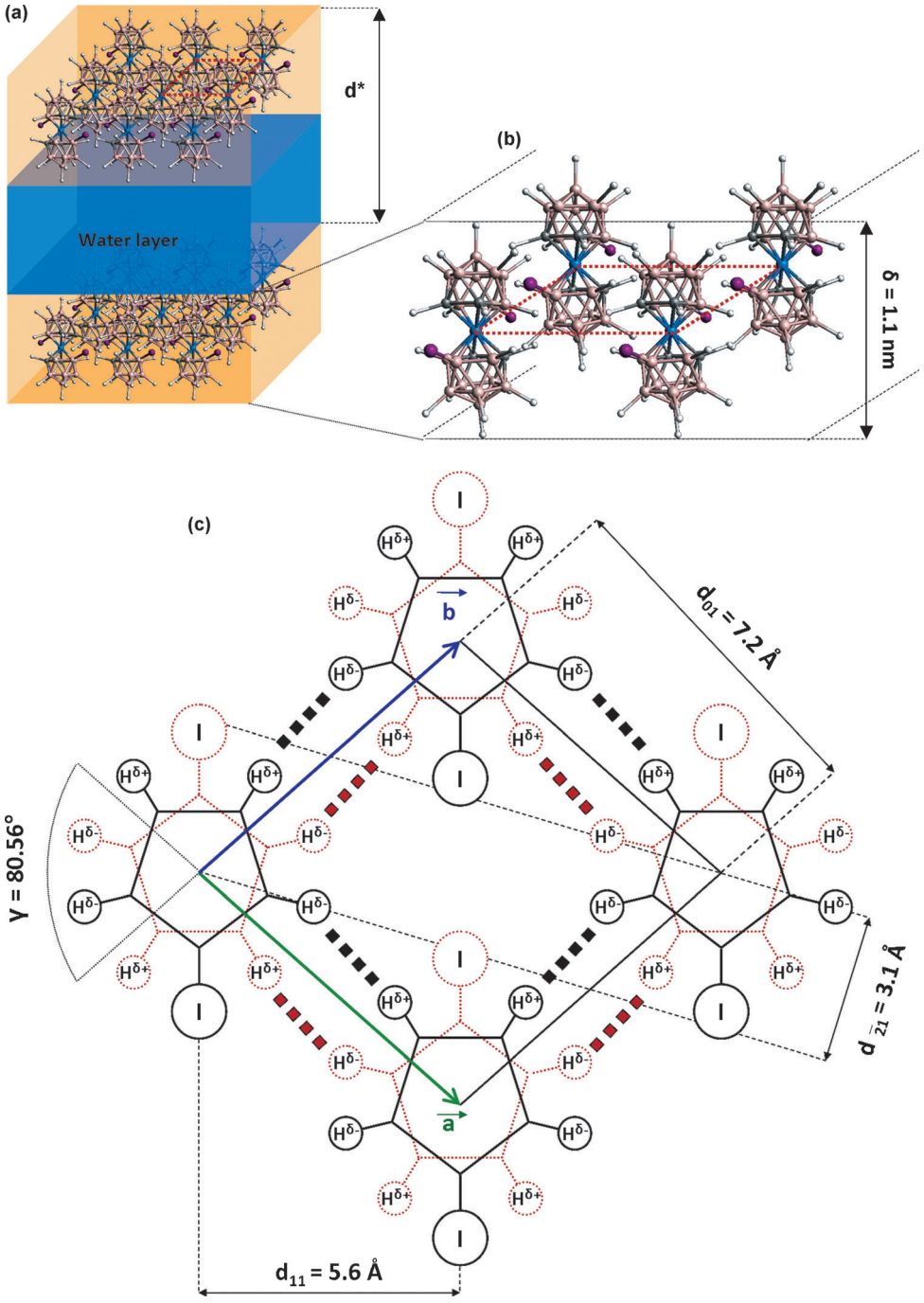

Figure 5. Molecular representation of the lamellae formed by I_2COSAN in water: a) lamellar phase showing smectic arrangements of I_2COSAN monomolecular layers and water layers, b) lateral view of the lamella and c) schematic representation crystal lattice of the 2D structure showing selected interatomic distances. Hydrogen bonds indicated by broken lines.

distance between $[I_2COSAN]^-$ molecules (6.6 Å) given by the broad peak position in the L_α phase at 9.4 nm^{-1}. Consequently the density in the film increases during the solid-to-liquid phase transition, like water does when it turns from ice into its liquid state, which is an indication for an intermolecular H-bond network being strongly involved in the structuration of the 2D I_2COSAN film. Note that the I_2COSAN density increases by about 29 % $(1-(A_{L\alpha})^{3/2}/(A_{L\beta})^{3/2})$ during the L_β–L_α transition whereas the density of water increases only by 8 % from ice to liquid water. This significant difference may be related to the large difference in the H-bond length between water, around 1.97 Å, and I_2COSAN. Moreover the increase in the interlamellar spacing while melting (Figure S2) may indicate that the I_2COSAN molecules also partly disorder out of plane disorder.

Further increase in the temperature leads to L_α–L_1 transition that shows a dramatic change in the aggregate curvature from plane interface to small nanometric micelles. Such a transition is ubiquitous in most surfactant binary phase diagrams.[13] During this transition the average molecular area further increases from 43 to 57.8 $Å^2$, calculated as the square of the average intermolecular distance between H[I_2COSAN] molecules (7.6 Å) a value determined from the broad peak position in the L_1 phase at 8.0 nm^{-1}. For H[COSAN] micelles the intermolecular peak position was found at higher q values, 10.8 nm^{-1} ($d = 0.56$ nm)[2] compared to 8.0 nm^{-1} ($d = 0.785$ nm) for $[I_2COSAN]^-$ the difference being explained by the presence of the two bulky iodine atoms that increases the distance between closest neighbor molecules. The increase in the molecular area from L_α to L_1 phase can be rationalized in terms of a decrease in the packing parameter, P[22] which is a geometrical parameter giving a relationship between the molecular structure and the aggregate state ($P = 1$ for plane structures, $P = 1/2$ for cylinders, and $P = 1/3$ for spheres). P is defined as $P = v/al$, with v, the molecular volume, a, the molecular area, and l, the molecular length. As v and l are constant, the temperature induced transition from L_α to L_1 phase is then controlled by the increase in a as noticed experimentally by the increase in the average distance between close neighbor molecules.

In conclusion, we have shown that the $[I_2COSAN]^-$ macro ion combines properties of purely organic surfactants and purely inorganic sheet systems, such as clays. Similarly to surfactants $H[I_2COSAN]$ self-assemble in layers that 1) form lyotropic lamellar phases in the concentrated regime, 2) that are able to bend into (closed) vesicles in the dilute regime, and that 3) show a transition from solid-like to liquid-like state on increasing temperature. On the other hand, lamellas formed by $H[I_2COSAN]$ are made of monomolecular sheets, such as clay systems, but with the sole difference that they are not covalently bound. The cohesive energy between $[I_2COSAN]^-$ ions, that leads to the lamella formation, originates presumably from intermolecular dihydrogen bonds whose formation is possible owing to the different polarity of the B–H bond vertexes in the $[I_2COSAN]^-$ cluster. Monolayers of $[I_2COSAN]^-$ are less rigid than purely inorganic covalently bound sheets so their bending is then accessible with thermal energy leading to the formation of vesicles which is not possible with clay systems. The formation of a lamellar phase seems to be a general property of metallabis(dicarbollide) systems as it could also be detected with H[COSAN] but at higher concentrations (see the SWAXS spectra Figure S6). This information on the intermolecular forces involved in the self-assembly of COSAN derivatives in water is essential for a rational design for their applications in many different fields, such as in the reprocessing of spent nuclear fuel,[23] in analytical chemistry as main component in ion-selective electrodes,[24] in solar cells design as fast redox shuttle,[25] in medicine as promising building block for drug design,[26] or in boron-neutron capture therapy.[27] The organic–inorganic hybrid lamellar phases studied could have potential applications as new liquid-crystal systems for display or memory storage if the cobalt center can be replaced with a magnetic atom, such as iron. The tunable oxidation state of the theta-shaped amphiphile metal[28] could also be used to design active nano-materials for sensing and for photonic applications.

Received: August 21, 2013

Keywords: amphiphiles · carboranes · hydrogen bonds · lamellar phases

[1] a) Y. Talmon, D. F. Evans, B. W. Ninham, *Science* **1983**, *221*, 1047 – 1048; b) C. R. Safinya, E. B. Sirota, R. F. Bruinsma, C. Jeppesen, R. J. Plano, L. J. Wenzel, *Science* **1993**, *261*, 588 – 591; c) E. W. Kaler, A. K. Murthy, B. E. Rodriguez, J. A. Zasadzinski, *Science* **1989**, *245*, 1371 – 1374; d) T. Zemb, M. Dubois, B. Deme, T. Gulik-Krzywicki, *Science* **1999**, *283*, 816 – 819; e) H. Shen, A. Eisenberg, *Angew. Chem.* **2000**, *112*, 3448 – 3450; *Angew. Chem. Int. Ed.* **2000**, *39*, 3310 – 3312; f) D. Volodkin, Y. Arntz, P. Schaaf, H. Moehwald, J. C. Voegel, V. Ball, *Soft Matter* **2008**, *4*, 122 – 130.

[2] P. Bauduin, S. Prevost, P. Farras, F. Teixidor, O. Diat, T. Zemb, *Angew. Chem.* **2011**, *123*, 5410 – 5412; *Angew. Chem. Int. Ed.* **2011**, *50*, 5298 – 5300.

[3] C. Tanford, *Science* **1978**, *200*, 1012 – 1018.

[4] Q. Wang, D. O'Hare, *Chem. Rev.* **2012**, *112*, 4124 – 4155.

[5] a) S. Hassan, W. Rowe, G. J. Tiddy, *Surfactant Liquid Crystals in Handbook of Applied Surface and Colloid Chemistry* (Ed.: K. Holmberg), Wiley, Chichester, **2001**, p. 465; b) S. Hyde, *Identification of Lyotropic Liquid Crystalline Mesophases in Handbook of Applied Surface and Colloid Chemistry* (Ed.: K. Holmberg), Wiley, Chichester, **2001**, pp. 299 – 332; c) W. Gelbart, A. Ben-Shaul, D. Roux. Micelles, *Membranes*, *Microemulsions*, *and Monolayers*, Springer, Berlin, **1994**.

[6] I. Amar-Yuli, D. Libster, A. Aserin, N. Garti, *Curr. Opin. Colloid Interface Sci.* **2009**, *14*, 21 – 32.

[7] a) R. Mezzenga, *Self-Assembled Food Mesophases.* Research Worlds—Focus on Food. Alimentarium Foundation Editions, **2009**; b) K. Larsson, *Curr. Opin. Colloid Interface Sci.* **2009**, *14*, 16 – 20.

[8] K. Na, M. Choi, W. Park, Y. Sakamoto, O. Terasaki, R. Ryoo, *J. Am. Chem. Soc.* **2010**, *132*, 4169 – 4177.

[9] H. Yao, I. Hatta, R. Koynova, B. Tenchov, *Biophys. J.* **1992**, *61*, 683 – 693.

[10] a) P. Farràs, E. J. Juárez-Pérez, M. Lepšik, R. Luque, R. Núñez, F. Teixidor, *Chem. Soc. Rev.* **2012**, *41*, 3445 – 3463; b) F. Teixidor, *J. Organomet. Chem.* **2009**, *694*, 1587 – 1587.

[11] P. Matejıcek, P. Cıgler, K. Prochazka, V. Kral, *Langmuir* **2006**, *22*, 575 – 581.

[12] P. Farras, C. Viñas, F. Teixidor, *J. Organomet. Chem.* **2013**, DOI: 10.1016/j.jorganchem.2013.03.039.

[13] R. G. Laughlin, *The aqueous phase behavior of surfactants*, Academic Press Limited, San Diego, **1994**.

[14] G. Menges, E. Haberstroh, W. Michaeli, E. Schmachtenberg, *Plastics Materials Science*, Hanser Fachbuchverlag, Leipzig, **2011**.

[15] M. Dubois, T. Zemb, *Langmuir* **1991**, *7*, 1352 – 1360.

[16] M. Morvan, D. Espinat, R. Vascon, J. Lambard, T. Zemb, *Langmuir* **1994**, *10*, 2566 – 2569.

[17] L. J. Michot, I. Bihannic, S. Maddi, S. S. Funari, C. Baravian, P. Levitz, *Proc. Natl. Acad. Sci. USA* **2006**, *103*, 16101 – 16104.

[18] J. C. P. Gabriel, F. Camerel, B. J. Lemaire, H. Desvaux, P. Davidson, P. Batail, *Nature* **2001**, *413*, 504 – 508.

[19] D. Gazeau, T. Zemb, M. Dubois, *Prog. Colloid Polym. Sci.* **1993**, *93*, 123 – 129.

[20] B. E. Warren, *Phys. Rev.* **1941**, *59*, 693 – 698.

[21] O. N. Kazheva, G. G. Alexandrov, A. V. Kravchenko, V. A. Starodub, I. A. Lobanova, I. B. Sivaev, V. I. Bregadze, L. V. Titov, L. I. Buravov, O. A. Dyachenko, *J. Organomet. Chem.* **2009**, *694*, 2336 – 2342.

[22] J. N. Israelachvili, D. J. Mitchell, B. W. Ninham, *J. Chem. Soc. Faraday Trans.* **1976**, *72*, 1525 – 1568.

[23] G. Chevrot, R. Schurhammer, G. Wipff, *J. Phys. Chem. B* **2006**, *110*, 9488 – 9498.

[24] A. I. Stoica, C. Viñas, F. Teixidor, *Chem. Commun.* **2009**, 4988 – 4990.

[25] T. C. Li, A. M. Spokoyny, C. X. She, O. K. Farha, C. A. Mirkin, T. J. Marks, J. T. Hupp, *J. Am. Chem. Soc.* **2010**, *132*, 4580 – 4583.

[26] a) E. Meggers, *Angew. Chem.* **2011**, *123*, 2490 – 2497; *Angew. Chem. Int. Ed.* **2011**, *50*, 2442 – 2448; b) J. Rak, B. Dejlova, H. Lampova, R. Kaplanek, P. Matejicek, P. Cigler, V. Kral, *Mol. Pharm.* **2013**, *10*, 1751 – 1759.

[27] E. L. Crossley, E. J. Ziolkowski, J. A. Coderre, L. M. Rendina, *Mini-Rev. Med. Chem.* **2007**, *7*, 303 – 313.

[28] M. F. Hawthorne, J. I. Zink, J. M. Skelton, M. J. Bayer, C. Liu, E. Livshits, R. Baer, D. Neuhauser, *Science* **2004**, *303*, 1849 – 1851.